Accuracy of Computational Chemistry Methods to Calculate Organic Contaminant Molecular Properties

Kevin Bonnot, Pierre Benoit, Sophie Hoyau, Laure Mamy, Dominique Patureau, Rémi Servien, Mathias Rapacioli, Fabienne Bessac

Accuracy of Computational Chemistry Methods to Calculate Organic Contaminant Molecular Properties

Dr. Kevin Bonnot[a],[b], Prof. Dr. Pierre Benoit[b], Dr. Sophie Hoyau[c], Prof. Dr. Laure Mamy[b], Prof. Dr. Dominique Patureau[a], Dr. Rémi Servien[a], Dr. Mathias Rapacioli[c], Dr. Fabienne Bessac[c],[d]*

[a] INRAE, Univ Montpellier, LBE, 102 avenue des Etangs, 11100, Narbonne, France.

[b] Université Paris-Saclay, INRAE, AgroParisTech, UMR ECOSYS 78850 Thiverval-Grignon, France.

[c] Université de Toulouse; Laboratoire de Chimie et Physique Quantiques (UMR 5626), UPS, CNRS; 118, route de Narbonne; F-31062 Toulouse, France.

[d] Université de Toulouse; INPT; Ecole d'Ingénieurs de Purpan; 75, voie du TOEC, BP 57611, F-31076 Toulouse Cedex 03, France.

*fabienne.bessac@irsamc.ups-tlse.fr

https://www.lcpq.ups-tlse.fr/spip.php?article1234

Abstract

The quantitative structure activity relationship (QSAR) methodology has been developed and extensively used to predict unknown environmental data for compounds that have not been experimentally studied yet. QSAR is based on a large series of descriptors: such as the number of atoms, the number of bonds… (descriptive), or based on the 2D structure of the molecule (connectivity indices…) or on its 3D structure (dipole moment, polarizability…). Among them, quantum-based 3D descriptors appear as promising tools to predict macroscopic environmental properties. For a set of 104 pharmaceuticals and personal care products, four quantum-based 3D descriptors (electric dipole moment, polarizability, HOMO energy and ionization potential) were calculated using different computational chemistry strategies involving a conformational search followed by local quenches within three different frameworks: density functional theory (DFT), semi-empirical Austin Model 1 (AM1) approach, and density functional based tight binding (DFTB). Comparing the results obtained using each framework highlights the necessity of a comprehensive conformational search and the use of an accurate potential for the local quenches. Using the combination of a global exploration through molecular dynamics with local quenches at B3LYP/6-31G* (DFT) allows the calculation of accurate and trackable quantum-based 3D descriptors.

Introduction

Pharmaceuticals and personal care products (PPCP) have been increasingly studied over the past twenty years. This emerging contaminants family contains diverse groups of organic compounds, named according to their use or biological response, such as antibiotics, hormones, anti-inflammatory drugs, antiepileptic drugs, blood lipid regulators, β-blockers, contrast media and cytostatic drugs for pharmaceuticals; antimicrobial agents, synthetic musk, insect repellents, preservatives, fragrance components and sunscreen UV filters for personal care products[1,2]. Understanding the fate and effects of PPCP in the environment is therefore essential from human and environmental health perspectives. However, due to the high number of substances and of their transformation products, their fate cannot be studied experimentally on a case-by-case basis[3]. Consequently, numerous tools using computational and statistical methods have been developed to predict unknown environmental data for compounds that have not been experimentally studied yet. Among them, Quantitative Structure Activity Relationships (QSAR) are based on the assumptions that the structure of the lowest-energy conformer of a molecule in the gas phase contains the features responsible for its physical and chemical properties despite the environmental and/or biological interactions, which inevitably modifies the conformation of the compound in use. For instance, QSAR has been used to predict the fate of various organic compounds[4–6]. Mamy *et al.*[6,7] have compiled many of these QSAR used to predict volatilization, transformation, etc. and have identified the common and generic structural parameters used in these equations. Forty common structural parameters, combining constitutional, topological, geometric, and electronic properties, were thus calculated for 500 organic compounds and transformation products, and implemented in the database of a recently developed clustering tool: TyPol (Typology of Pollutants). TyPol allows the classification of organic compounds according to both their overall behavior in the environment (characterized through mobility, persistence, volatility…) and ecotoxicological effects (bioconcentration factor, no observed effect concentration…), and to the set of the 40 structural parameters[8]. These latter gather molecular descriptors such as the number of atoms, the number of bonds… (descriptive) or based on the 2D structure of the molecule (connectivity indices…) or on its 3D structure (dipole moment, polarizability…). Most molecular descriptors used in TyPol are provided by the Dragon software[9] but the calculation of the 3D quantum-based descriptors that appear especially powerful to predict macroscopic environmental properties[6,10], needs to use other softwares and methods. Some properties have already been computed for organic molecules either on few 3D quantum based descriptors or on relatively small molecules [11–13]. Moreover, the level of theory used to compute 3D quantum-based descriptors influences the obtained values by two ways: (i) the structural conformation of the lowest-energy isomer; (ii) the accuracy of the methods to compute the set of quantum descriptors. Semi-empirical approaches such as Austin Model 1 (AM1) or PM3 (Parametric Method 3) are often used to predict the physicochemical properties of a family of molecules[14,15] or their behavioral parameters[6]. The main advantage of those approaches relies on their low computational costs (time and memory). For example, up to now, AM1 is used in TyPol after a conformational search made “by hand”, to evaluate the 3D quantum descriptors listed in the database[8].

Therefore, the objective of this work was to compare several computational chemistry strategies to calculate the quantum descriptors of organic compounds from the case study of 104 PPCP implemented in TyPol. The update of the database will be performed by non-computational chemists. Thus, an easy-to-use program chain will be implemented. In this paper, the selected potentials will be first described, followed by the impact of the conformational search method on the determination of

the lowest-energy isomer. Then, the effect of the potential used into the quantum descriptor calculation is discussed. Afterwards, a comparison between the quantum descriptor values presently in Typol and the ones computed at the recommended level is done. Then, the effect of the temperature on the set of quantum descriptors is studied using a mean value over the five lowest-energy isomers with weights based on the Boltzmann distribution. Finally, connections between the quantum and the non-quantum descriptors are attempted.

Materials and Methods

Computational Chemistry Methods

Three different frameworks were used for the quantum calculation of the molecular electronic structures of PPCP in the gas phase:

- the density functional theory (DFT);
- an approximated scheme of DFT, the Density Functional based Tight Binding (DFTB);
- a semi-empirical method (Austin Model 1, AM1).

DFT. Within the DFT framework,[16] [17] the calculations were performed using the B3LYP hybrid functional[17–19]. Two basis sets have been used in this work. On the one hand, the 6-31G* basis set[20] [21] [22] was called "basis1" (see SI for more details). On the other hand, the 6-311+G(2d,2p) basis set [23] [24,25] [22] was denoted "basis2" (see SI for more details). In previous work on similar molecules (pesticides), the authors showed that the B3LYP/basis1 level is a nice compromise between accuracy and tractability to compute geometries with respect to correlated methods such as MP2 and CCSD(T). However, using basis1 or basis2 could slightly change the order of the isomers close in energy.[26,27] The calculations were run using Gaussian09 package[28].

DFTB. The mathematical expression for the DFTB energy is derived from DFT first principle theorems and is parameterized from DFT reference calculations[29–31],[32–34]. In this work, we have used the third order version of DFTB [32–34] (simply labelled DFTB in the following) with the 3-ob parameters set[34] (downloaded from the www.dftb.org website), a correction for the hydrogen bond interactions (see Gaus et al.[33]) and an empirical long-range dispersion correction[35]. We used a Fermi electronic distribution (temperature of 500 K) to avoid convergency issues. It was however removed (Fermi temperature set to 0 K) for the final local optimization steps (see below). The polarizabilities were obtained from the scheme proposed by Witek *et al.*[36]. All DFTB calculations were performed with the deMonNano code[37] (see SI for more details).

AM1. AM1 is a parametric quantum mechanical molecular model[38,39]. The parameterization of the model was carried out with a particular attention on dipole moments, ionization potentials, and geometries of molecules[38,39]. Up to now, AM1 is used in TyPol to compute 3D quantum descriptors.

Strategy

Two strategies were compared to obtain the lowest-energy isomer structures of the 104 PPCP. The first one, up to now used in TyPol, relies on angle and dihedral rotations made "by hand" to generate, for each molecule, a guessed geometry, which is further optimized locally, making use of the eigenvalue-following algorithm[40–42] combined with the AM1 potential. These structures will be

labelled H_AM1 (for “by hand” designed + AM1 optimization) in the following. The second one relies on a combination of global exploration through molecular dynamics (MD) with periodic local quenches to improve the conformational search.

Molecular Dynamics

The MD exploration is performed at the DFTB level at high temperature to ensure that barriers separating basins associated to various conformers can easily be overcome (Figure 1a).

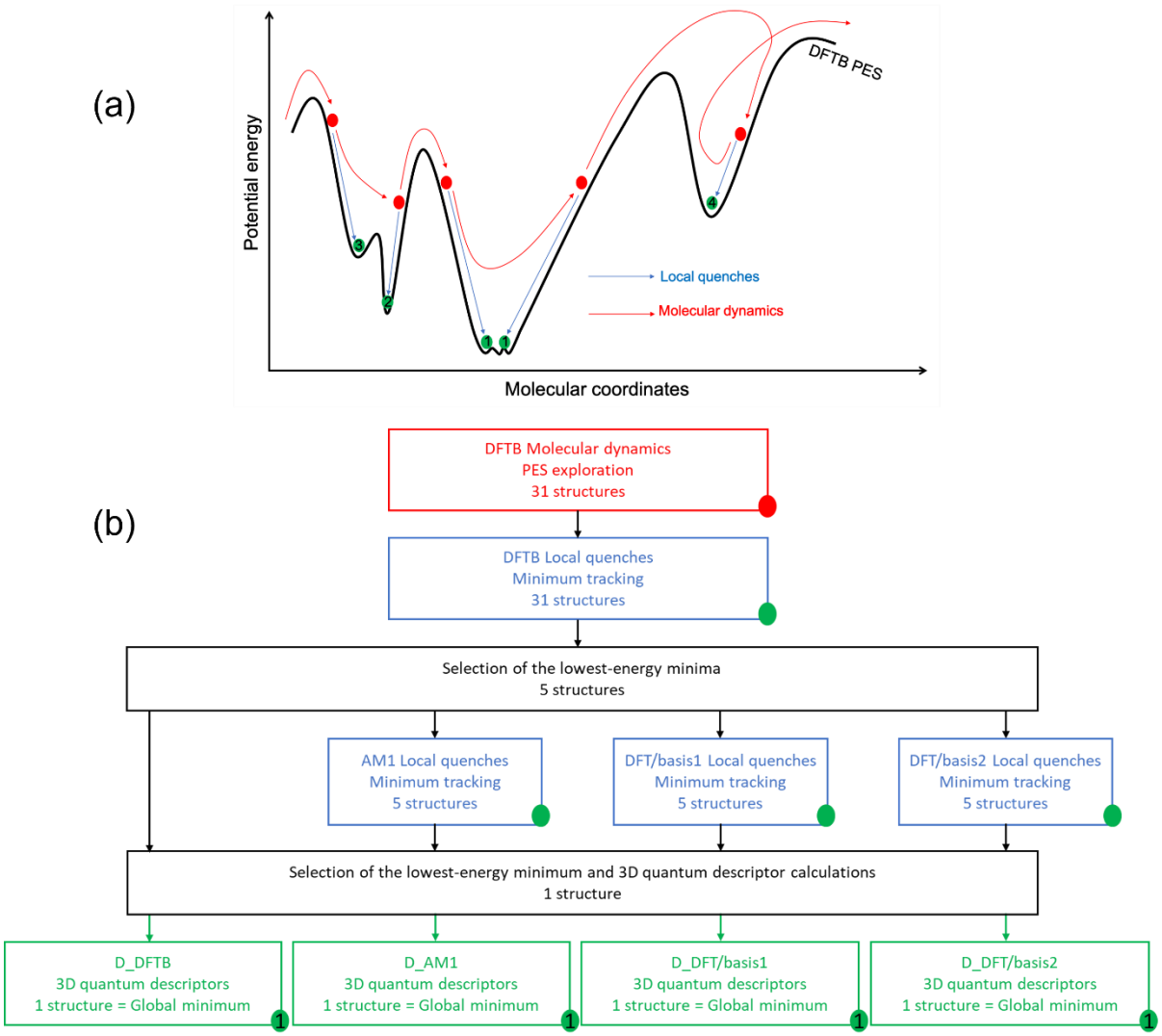

Figure 1. (a) Schematic representation of the potential energy surface (PES) explored by DFTB molecular dynamics simulations for a molecular system. (1) is the global minimum; (2), (3) and (4) are local minima. In red, PES structures reached by the DFTB/MD exploration; in blue, path followed by the quench (geometry optimization) leading to the closest local minimum. (b) Graphical representation of the steps followed for the four molecular dynamic (MD) based strategies to calculate the quantum descriptors of organic compounds from the case-study of 104 PPCP. Red and green dots have the same meaning as in (a).

The temperature was maintained through a chain of 5 Nose Hoover thermostats at 800 K associated to an energy exchange frequency of 300 cm^{-1}. Ten ps were simulated for each molecule starting from a guessed structure. The timestep was set to 1 fs, which would probably be too large to extract properties from such simulations but sufficient for the exploration purpose of the present work.

Local Quenches

Thirty-one structures were then extracted corresponding to snapshots equally spaced along the MD run. The latter were further optimized at the DFTB level (conjugated gradient) and the five lowest-energy ones were selected for further local optimizations at the AM1, B3LYP/basis1 and B3LYP/basis2 levels of theory using the Berny algorithm[43]. These structures will be labelled D_DFTB, D_AM1, D_DFT/basis1 and D_DFT/basis2 in the following, D_ accounting for the (DFTB/MD + quenches) exploration scheme followed by the level of theory used for the final local optimization procedure. The various strategies are summarized in Table I and Figure 1b.

Table I. Computational chemistry strategies used in this work with the associated labels. The first part of the label refers to the potential energy surface (PES) exploration: H_ by hands or D_ using DFTB3 molecular dynamics simulations (MD). The second part of the label refers to the local optimization level.

LABEL	*PES exploration*		*Local optimization*
	By hand	*MD*	
H_AM1	×		AM1
D_AM1		×	AM1
D_DFTB		×	DFTB3
D_DFT/basis1		×	B3LYP/6-31G*
D_DFT/basis2		×	B3LYP/6-311+G(2d,2p)

Properties

This work focuses on four 3D quantum-based chemical descriptors frequently used in QSAR, three of them already present in TyPol[6,8]: the dipole moment (Debye), the polarizability ($Bohr^3$), the HOMO energy (eV); and the ionization potential (eV).

The ionization potential IP (electron-Volt) is the minimal energy necessary to extract one electron from a gas phase molecule in its neutral fundamental state. IP is the energy difference between the cation (formed after the electron extraction) and the neutral molecule: $IP = E_{cation} - E_{neutral}$. In this work, we only consider the vertical IP, *i.e.*, E_{cation} is the energy of the cation at the optimized neutral geometry. In practice, IP can be computed by direct or indirect methods. In the indirect method, E_{cation} and $E_{neutral}$ are computed from two independent calculations. The direct method relies on the Koopman's Theorem (KT)[44], which stipulates that the first IP equals the opposite value of the HOMO (Highest Occupied Molecular Orbital) energy of the neutral molecule: $IP_K = - E_{HOMO}$ (electron-Volt). Differences exists between the two approaches. The KT considers that the electron is extracted from the HOMO.

Then, it only considers the HOMO energy and neglects the electronic reorganization after extracting the electron (see SI for more details[45],[46–50]).

Dataset

The dataset consisted of 104 PPCP. The most represented use families are antibiotics (34% of the data set), antidepressants (8%), fragrance components (8%), hormones and NSAIDs (Non-Steroidal Anti-Inflammatory Drugs) (7%). At the H_AM1 level, dipole moments, polarizabilities, and HOMO energies were calculated for the 104 PPCP (the complete molecule set). At the D_AM1, D_DFTB, and D_DFT/basis1 levels, dipole moments, polarizabilities, HOMO energies, and ionization potentials were obtained for the 104 PPCP. At the D_DFT/basis2 level, dipole moments, polarizabilities, HOMO energies, and ionization potentials were determined for 100 PPCP. For four molecules: azithromycin, erythromycin, oleandomycin and roxithromycin; there were missing values because local geometry optimizations did not converge.

Results and Discussion

Conformational Search

For extended molecules presenting very soft modes, it is worth noticing that the basins of the PES often present multiple isomers very close in energy and differing by small geometrical atomic displacements (Figure 1a). The fine details of these wells are sensitive to the level of theory used to describe the PES. Therefore, it is not always an easy task to state if two structures optimized with two different levels of theory correspond to the same isomer: it requires some degree of arbitrariness in the selected procedures, which will be detailed in the following.

First, the results from the strategies involving a DFTB/MD exploration, namely D_AM1, D_DFTB, D_DFT/basis1 and D_DFT/basis2, are discussed. The five lowest-energy isomers obtained with the D_DFTB strategy were labelled according to their energetic position (1 to 5) before further optimization at the AM1 or DFT levels of theory. If two strategies found the same isomer name (same number) for their lowest-energy isomers, we considered that they agree on the structure of the most stable isomer. This approach was called the identification procedure 1 (IdP1). The 104 molecules were classified within five groups labelled by **0**, **1**, **2**, **3** and **4** indices as follows (these groups are **exclusive**, see Table SI):

- If the lowest-energy isomer has the same name with D_AM1, D_DFTB, D_DFT/basis1 and D_DFT/basis2 strategies, the molecule is indexed **1**;
- If the lowest-energy isomer has the same name only for D_DFTB, D_DFT/basis1 and D_DFT/basis2 strategies, the molecule is indexed **2**;
- If the lowest-energy isomer has the same name for D_DFT/basis1 and D_DFT/basis2 strategies but not with the D_DFTB strategy, the molecule is indexed **3**;
- If the lowest-energy isomers at D_DFT/basis2 and D_DFT/basis1 strategies have different names, the molecule is indexed **4**;
- for four molecules, the D_DFT/basis2 local geometry optimizations did not converge and they were indexed **0**.

Indices **0**, **1**, **2**, **3** and **4** gathered 3.8 %, 27.9%, 15.4%, 33.7% and 19.2% of the molecule set, respectively. In other words, the four levels of theory led to the same most stable structure after local optimization of the same five isomers for only 27.9% of the molecule set (index **1**). For 15.4% of the 104 compounds, only the DFT like levels of theory, namely D_DFTB, D_DFT/basis1 and D_DFT/basis2 gave the same lowest-energy isomer name (index **2**). For 19.2 % of the set, changing the basis for the DFT/B3LYP calculations, led to different most stable isomers (index **4**). These results point out the strong dependence of the identified most stable structures on the choice of the potential. The largest correspondence between the various computational methods was obtained for D_DFT/basis1 and D_DFT/basis2, which agreed for 80% of the molecule set (Table II). The agreement with the most accurate strategy, D_DFT/basis2, drops to less than 50% when the local optimization was performed at the DFTB or AM1 levels of theory (Table II), showing that working within the density functional theory framework brings a decisive and unquestionable improvement. D_DFTB and D_AM1 present similar abilities (between 44 and 50%) at recovering the D_DFT/basis2 or DFT/basis1 lowest-energy minima (Table II). It must be underlined that both parametrized strategies, D_DFTB and D_AM1, only agree for 49% of the molecule set (Table II).

Table II. Percentages of isomer correspondences among the studied computational chemistry strategies. The percentages written in black correspond to when both methods found the same isomer number for their lowest-energy isomers. The percentages in red correspond to when both methods found the same total energy (total energy difference < 10^{-3} au) when the structure of the lowest-energy isomer of the most accurate method is reoptimized at the least accurate level of theory.

	H_AM1	*D_AM1*	*D_DFTB*	*D_DFT/basis1*	*D_DFT/basis2*
H_AM1		36	35	28	32
D_AM1			49/59	46/54	44/57
D_DFTB				50/50	48/52
D_DFT/basis1					80/90
D_DFT/basis2					

The identification procedure IdP1 only applies to strategies involving the DFTB/MD exploration as a first step. Consequently, as the isomer structures obtained at the H_AM1 level are not products of the MD exploration, the isomer numbering is not comparable to the other methods (D_) arising from the MD exploration. To allow comparison with the H_AM1 strategy, we defined a second procedure to compare the most stable isomers found by the two strategies: the structure of the lowest-energy isomer of the most accurate method (M1) was reoptimized at the least accurate level of theory (M2) giving EtotM1. Then, we compared this energy to EtotM2, the total energy of the lowest-energy isomer at M2 level by calculating the total energy difference ΔEtot = EtotM1-EtotM2. If $|\Delta Etot| < 10^{-3}$ a.u., it was considered that both strategies found the same lowest-energy isomer. This new identification strategy, IdP2, was used to provide the red number in Table II.

When both ways to evaluate isomer correspondences (IdP1 and IdP2) were possible, IdP1 always gave percentages of correspondence lower than those of IdP2 although presenting the same trend. The largest difference is of 13 points (D_AM1 versus D_DFT/basis2), the smallest of 0 point (D_DFTB versus D_DFT/basis1). Going vertically down through a column the percentages increase a lot (variations up to 58%), whereas going horizontally left to right through a line, they remain mostly unchanged ($|\text{variations}| \leq 8\%$).

H_AM1 had the lowest correspondence rates with any of the other methods, below 36%, meaning that the MD PES exploration has provided a tremendous improvement in the conformational search and in particular, the identification of the lowest-energy isomer (Table II). It was particularly striking to obtain the poor agreement of 36%, when comparing H_AM1 and D_AM1 because the two methods differed only by the MD exploration prescreening, and the final local optimization was performed at the same level (AM1). In addition, when going from H_AM1 to D_AM1, the agreement with D_DFT/basis1 increases from 28 to 54 % (from 32 to 57 % for the agreement with D_DFT/basis2) (Table II).

As a conclusion, the MD PES exploration is mandatory due to the multiple minima exhibited by the PES on such extended molecules. Moreover, facing the lack of experimental data for the molecules of the set under study, comparisons will be made with respect to the highest level of theory of this study, D_DFT/basis2. However, comparing to experimental results, Hait and Head-Gordon showed that B3LYP with aug-pc-4, a polarization consistent basis set, gave 6.98% and 6.24% root-mean-square relative errors in dipole moments and polarizabilities, respectively when CCSD(T) gave 3.95% and 1.62% [12,13]. Their databases contained 132 (polarizability) and 200 (dipole moment) relatively small molecules (6 atoms max), while we deal with 104 compounds having between 16 and 134 atoms. Thus, our calculations at the DFT/basis2 level have already been very heavy given the size of the molecules. A reference level as CCSD(T) associated with a large basis set is simply not feasible for most of our molecules, again given their size.

Effects of the Computational Chemistry Methods on the Values of 3D Quantum Descriptors

As the influence of the computational method on the value of the 3D quantum descriptors was determined considering the D_DFT/basis2 strategy, only the matching molecules at both levels were considered (IdP1): 29 molecules for D_AM1 (index **1**), 45 molecules for D_DFTB (indices **1** and **2**) and 80 molecules for D_DFT/basis1 (indices **1**, **2** and **3**). Each quantum descriptor computed at D_DFT/basis2 level was compared to the descriptor computed at either D_AM1 or D_DFTB or D_DFT/basis1 (Figure 2 and Table III).

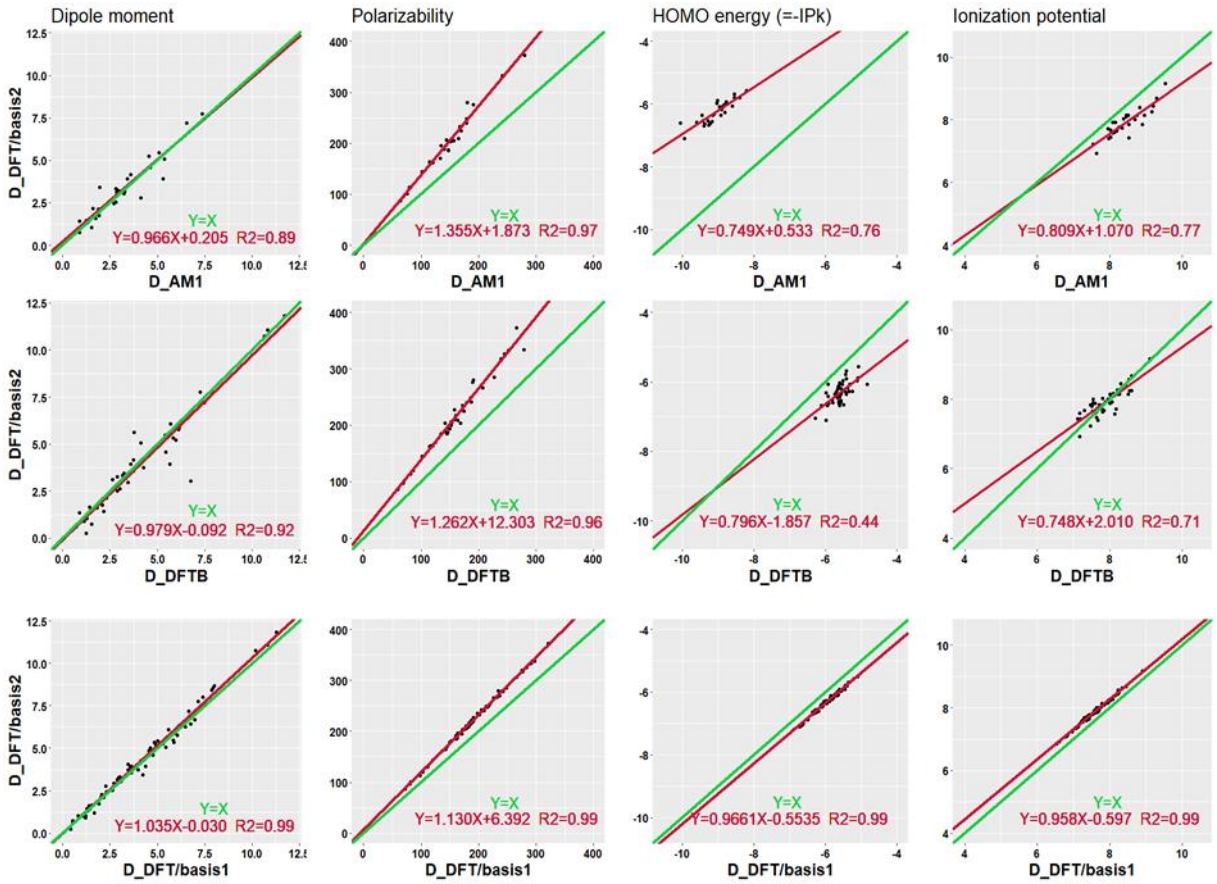

Figure 2. For the following quantum descriptors: dipole moment (Debye), polarizability (Bohr^3), HOMO energy (= -IP_K) (eV) and ionization potential (eV); straight lines in red are confronting D_DFT/basis2 results on the vertical axis to D_AM1, D_DFTB and D_DFT/basis1 results. On each graph, the equation, y=ax+b, of the linear regression line is written in red with the corresponding R^2 regression coefficient, while the green straight line represents the first bisector: y=x. The set of molecules used to produce the graphs were: (i) index **1**, for D_AM1 versus D_DFT/basis2 (29 molecules); (ii) indices **1** and **2** for D_DFTB versus D_DFT/basis2 (45 molecules); (iii) indices **1**, **2** and **3** for D_DFT/basis1 versus D_DFT/basis2 (80 molecules). The indices are defined in **Results and Discussion**.

Table III. Relative absolute errors (%) (mean, median, minimum, and maximum) for four 3D quantum descriptors (dipole moment, polarizability, HOMO energy (= $-IP_K$) and IP, ionization potential) calculated at D_AM1, D_DFTB and D_DFT/basis1 in comparison to the highest level of theory of this study, D_DFT/basis2. The set of molecules used to produce the numbers were: (i) index **1**, for D_AM1 versus D_DFT/basis2 (29 molecules); (ii) indices **1** and **2** for D_DFTB versus D_DFT/basis2 (45 molecules); (iii) indices **1**, **2** and **3** for D_DFT/basis1 versus D_DFT/basis2 (80 molecules). The indices are defined in **Results and Discussion**.

		Dipole Moment	*Polarizability*	*HOMO energy* $= -IP_K$	*Ionization Potential IP*
Mean	*D_AM1*	15	27	45	7
	D_DFTB	25	26	11	2
	D_DFT/basis1	9	14	6	4
Median	*D_AM1*	11	27	45	7
	D_DFTB	12	26	11	2
	D_DFT/basis1	7	14	6	4
Min	*D_AM1*	1	21	39	2
	D_DFTB	0	16	3	0
	D_DFT/basis1	0	12	4	2
Max	*D_AM1*	48	36	53	15
	D_DFTB	393	32	20	7
	D_DFT/basis1	65	18	8	5

For the dipole moment, D_DFT/basis2 vs. D_DFT/basis1 led to the best correlation coefficient (R^2 = 0.99). D_DFTB gives more dispersion (R^2=0.92) than D_DFT/basis1, and D_AM1 led to a correlation coefficient (R^2=0.89) lower than those of D_DFTB and D_DFT/basis1. At the same time, the slope the closest to one (a=0.979) was obtained with D_DFTB but the y-intercept the closest to zero was found for D_DFT/basis1 (b=0.030). Table III shows that, on average, the absolute values obtained for the dipole moment are better described at the D_DFT/basis1 level than at D_AM1 or D_DFTB levels. The average relative error is of 9% in D_DFT/basis1 compared to D_DFT/basis2 with a maximum of 65% and a minimum of 1%.

Concerning polarizability, the three methods underestimated the values with respect to D_DFT/basis2 as shown by the deviation from the first bisector. D_DFT/basis1 was the best method to reproduce polarizability (R^2=0.99, a=1.130). D_DFTB and D_AM1 also performed well (R^2=0.96 and 0.97 respectively) but led to a greater underestimation than D_DFT/basis1. The closest y-intercept to zero (b=1.873) was obtained with D_AM1. Again, according to Table III, D_DFT/basis 1 is the best method to reproduce the absolute values of polarizability. With respect to D_DFT/basis2, the relative errors on this descriptor are only 14% in average with a maximum of 18% and a minimum of 12%.

D_DFT/basis1 allowed the best determination of IP_K (= - E_{HOMO}) (R^2=0.99) although slightly underestimating IP_K comparing to D_DFT/basis2 (a=0.9661 and b=-0.5535<0). D_DFTB showed an

important dispersion (R^2=0.44) while it slightly underestimated the IP_K values. D_AM1 strongly overestimated IP_K for all the molecules of this set with an intermediate dispersion (R^2=0.76) (index **1**, 29 molecules). The average relative error made on IP_K in D_DFT/basis1 compared to D_DFT/basis2 is only 6% (Table III), a value is clearly lower than those obtained for D_AM1 (45%) and D_DFTB (11%).

For IP (computed with the indirect method), D_DFT/basis1 was the most efficient method (R^2=0.99) leading to a small underestimation of the values. D_DFTB showed a larger dispersion (R^2=0.71) with small over- or under- estimations while D_AM1 led to a comparable one (R^2=0.77) and overestimated IP values. The lowest average relative error regarding the IP evaluation with respect to D_DFT/basis2 (Table III) is obtained at the D_DFTB level (2%) but the performance of D_DFT/basis1 is almost equivalent (4%). However, with D_DFTB, the IP is either underestimated or overestimated, depending on the molecule, whereas with D_DFT/basis1, IP is systematically overestimated (Figure 2). Consequently, D_DFTB can hardly be used to predict IP trends on the opposite to D_DFT/basis1.

Finally, D_DFT/basis1 was the preferred method to compute the quantum descriptors as it gave the best regression coefficients (Figure 2) for all quantum descriptors and the smallest average relative errors (Table III) for all quantum descriptors except IP, with respect to D_DFT/basis2. Moreover, the computations are more tractable with D_DFT/basis1 than with the highest computational level (for local quench plus frequency calculations between 2.5 and 13 times more CPU time depending on the molecules). Consequently, the D_DFT/basis1 strategy can be recommended to calculate 3D quantum descriptors.

Moreover, for the molecules indexed 1, for which the four levels of theory led to the same most stable structure (27.9% of the molecule set), computing the lowest-energy isomer (local quench plus frequency calculation) at AM1 is between 91 and 1436 times faster than at DFT/basis1, and between 1204 and 34 425 times faster than at DFT/basis2. Local quench plus frequency calculations for the lowest-energy isomer lasted between 2 and 73 seconds (~1 minute) at AM1, between 441 and 70 738 seconds (~20 hours) at DFT/basis1, and between 5 178 and 1 401 534 seconds (~16 days) at DFT/basis2. Thus, a conformational search through molecular dynamics (D_) followed by local quenches at DFT/basis1 was the best compromise to reach accuracy and a reasonable computational cost.

H_AM1 versus D_DFT/basis1

After discussing separately, the effect of a global exploration and the choice of a potential to compute the quantum descriptors, we shine a light on the comparison between the previously implemented strategy in TyPol, namely H_AM1, and the new recommended strategy D_DFT/basis1. The quantum descriptor values determined by the H_AM1 strategy (presently in the TyPol database) and those calculated using D_DFT/basis1 strategy were compared (Figure S1) for the set of molecules with indices **1**, **2**, **3** and **4** (100 molecules). D_DFT/basis1 and H_AM1 quantum descriptors are discussed with respect to those computed at the D_DFT/basis2 level (see Figure 3a and 3b, respectively).

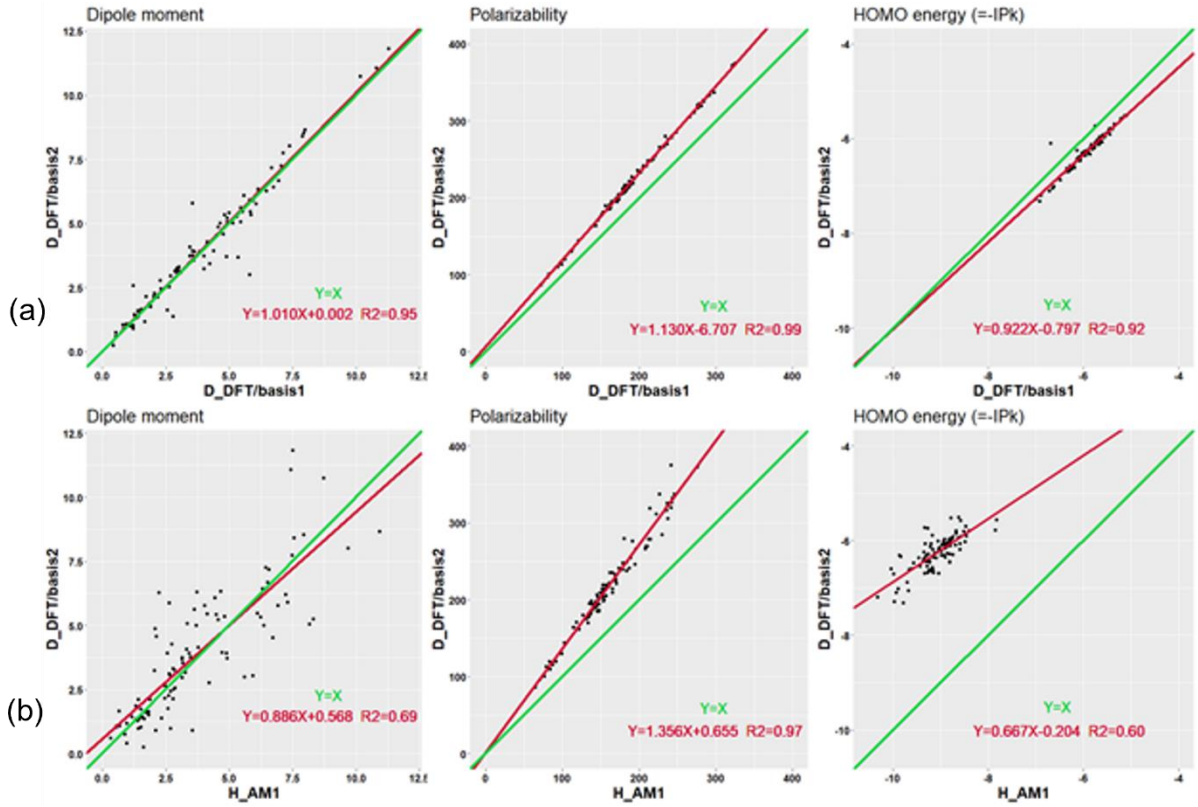

Figure 3. For the following quantum descriptors: dipole moment (Debye), polarizability (Bohr^3) and HOMO energy (= -IP_K) (eV); straight lines in red are confronting D_DFT/basis2 results on the vertical axis to: (a) D_DFT/basis1 results; (b) H_AM1 results. On each graph, the equation, y=ax+b, of the linear regression line is written in red with the corresponding R^2 regression coefficient, while the green straight line represents the first bisector: y=x. Only the set of molecules with indices **1**, **2**, **3** and **4** (100 molecules) was used to produce the graphs. The indices are defined in **Results and Discussion**.

For the dipole moment calculation, D_DFT/basis1 best matched D_DFT/basis2 (a=1.01, b=0.002) while less satisfactory results were obtained with H_AM1 (a=0.886, b=0.568) (Figure 3). In addition, the dispersion was significantly lower for D_DFT/basis2 vs. D_DFT/basis1 (R^2 = 0.95 > R^2 = 0.69 for D_DFT/basis2 vs. H_AM1) (Figure 3). Therefore, dipole moment values as listed in TyPol will be substantially improved using the D_DFT/basis1 strategy. As a set of 100 PPCP molecules was considered, the dispersion was more important than those observed on Figure 2 because only similar isomers according to IdP1 were selected (29 molecules D_DFT/basis2 vs. D_AM1; see **Effects of the Computational Chemistry Methods on the Values of 3D Quantum Descriptors**): R^2 = 0.89 for D_DFT/basis2 vs. D_AM1, and R^2 = 0.99 for D_DFT/basis2 vs. D_DFT/basis1. The differences originate from the molecular conformation, which was not the lowest in energy for many molecules using H_AM1 compared to D_AM1 (69 molecules D_DFT/basis2 vs. H_AM1 and 57 molecules D_DFT/basis2 vs. D_AM1). It should be noted that the dipole moment strongly depends on the molecular conformation. Thus, a global exploration (D_) is needed to properly compute dipole moment values (see also **Temperature effects**).

For the polarizability, the dispersions obtained with D_DFT/basis2 vs. H_AM1 and D_DFT/basis2 vs. D_DFT/basis1 were acceptable (R^2=0.97 and 0.99, respectively) (Figure 3). Indeed, the polarization,

depending on the size of the electronic cloud, is quite unchanged when the conformation of the molecule varies. This explains the small dispersion observed with D_DFT/basis2 vs. H_AM1. However, as mentioned in the previous section, all methods significantly underestimate polarizabilities with respect to the D_DFT/basis2 level (Figure 3). There was a clear underestimation of the polarizabilities calculated at H_AM1 (a=1.356 and b=0.655) and to a lesser extent at D_DFT/basis1 (a=1.130 and b=-6.707), compared to D_DFT/basis2 (Figure 3), which could be partly corrected by including atomic polarizabilities as implemented in the MOPAC package[8] but not in the Gaussian one. Up to now, TyPol quantum descriptors were calculated at the H_AM1 level of theory with the MOPAC package. Polarizabilities listed in TyPol are corrected and then accurate[a]. To compare polarizabilities computed with H_AM1 presently listed in TyPol to the other strategies, we calculated polarizabilities on H_AM1 structures via Gaussian package.

As explained in **Materials and Methods**, the ionization potential can be computed using the HOMO energy (= -IP_K, Koopman's Theorem). The AM1 potential led to a large overestimation of IP_K (D_AM1 on Figure 2). A huge overestimation of IP_K was observed for H_AM1 (a=0.667 and b=-0.204, R^2=0.60, Figure 3b) but an improved agreement was found for D_DFT/basis2 vs. D_DFT/basis1 (a=0.922 and b=-0.797, Figure 3a) leading also to a correlation coefficient close to one: R^2=0.916 (Figure 3). Indeed, the HOMO energy depends on the conformation of the molecule, so the dispersion is larger with H_AM1 considering the whole set of molecules (R^2=0.60 D_DFT/basis2 vs. H_AM1) than considering only 29 molecules (R^2=0.76 D_DFT/basis2 vs. D_AM1, Figure 2). Finally, the HOMO energy computed with AM1 could not be used to compute properly the ionization potential. We suggest replacing IP_K computed at the AM1 level by D_DFT/basis1 IP_K. Moreover, for a better accuracy of IP values, the indirect method using the cation and the neutral species energies is recommended (see discussion below, **Results and Discussion**).

As a conclusion, the H_AM1 strategy could lead to a reasonable calculation of polarizabilities if atomic corrections were added. However, the determination of accurate dipole moments and IP_K implies to make a more comprehensive conformational search through molecular dynamics (D_), and to use a higher level of theory for the local optimizations such as DFT/basis1 or DFT/basis2.

In addition, to evidence the potential to be chosen for 3D quantum molecular descriptor calculation, the absolute errors of the three different levels D_AM1, D_DFTB and D_DFT/basis1 were compared with respect to the D_DFT/basis2 values for each quantum descriptors under investigation in this work (Figure 4).

[a]MOPAC[51] manual specifies that "Polarizability volumes calculated using NDDO methods are too low by about 30%." "In 2004, the polarizability volume reported was modified by the use of additive corrections." "For normal organic compounds, the average error in polarizability should be less than 2%." http://openmopac.net/index.html

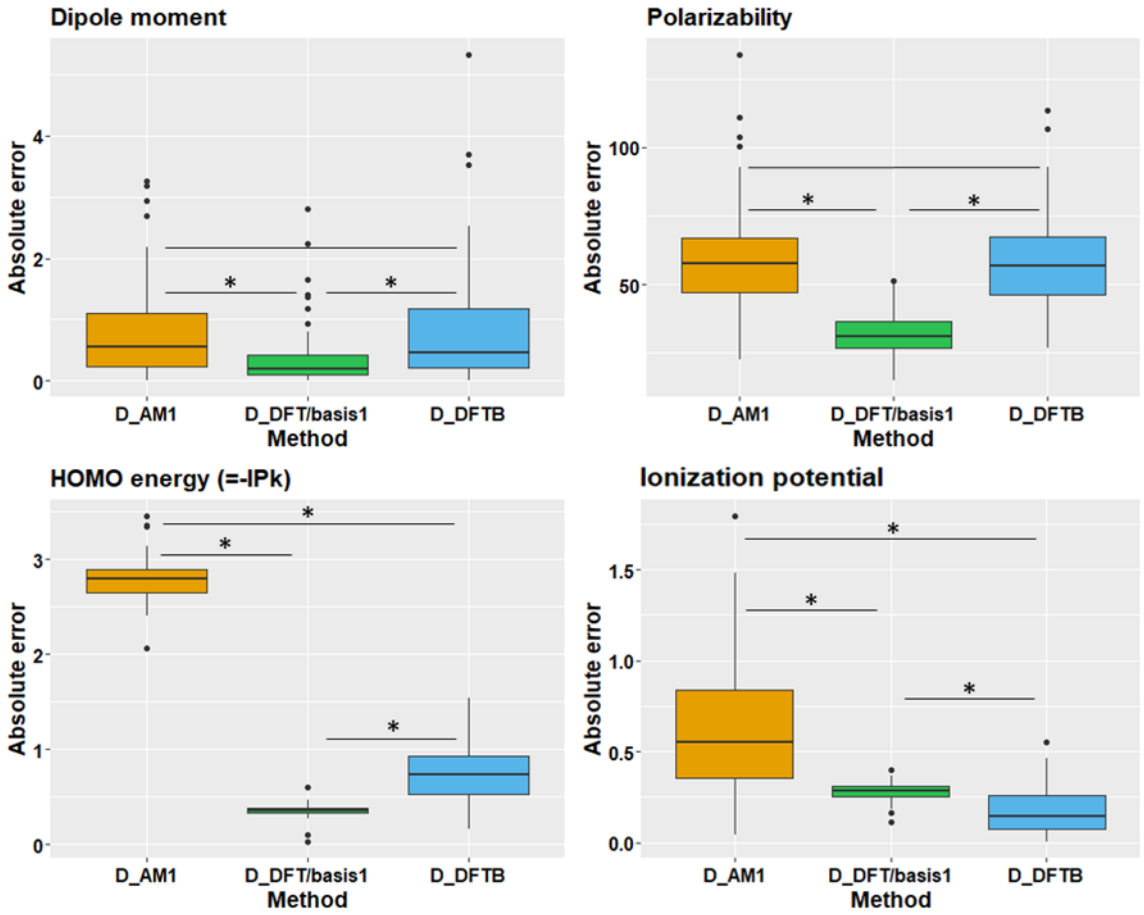

Figure 4. For the following quantum descriptors: dipole moment (Debye), polarizability (Bohr^3), HOMO energy (eV) and IP, ionization potential (eV), absolute error between D_AM1, D_DFTB and D_DFT/basis1 results and D_DFT/basis2 ones are plotted using boxplots. Only the set of molecules with indices **1**, **2**, **3** and **4** (100 molecules) was used to produce the graphs. Kruskal-Wallis and Dunnett test were performed to evaluate the difference between the methods (*: p-value< 0.001, hypothesis: the methods are significantly different). The indices are defined in **Results and Discussion**.

For the dipole moment, polarizability and HOMO energy, D_DFT/basis1 gave lower errors than D_AM1 and D_DFTB. Moreover, those errors were statistically different (* in Figure 4). For the ionization potential, all levels gave errors statistically different from each other but D_DFTB gives the lowest mean absolute errors compared to D_DFT/basis2. However, one must keep in mind that, as seen in the previous section, D_DFT/basis1 has the advantage to systematically overestimate the ionization potential values compared to D_DFT/basis2, while respecting the IP ordering of the various molecules, and could be used in a QSAR scheme where it is mandatory to respect the trends. On the opposite, D_DFTB over- or underestimates those values depending on the molecule, preventing its use to correlate IP to macroscopic properties.

Moreover, for the molecules indexed **1**, for which the four levels of theory led to the same most stable structure (27.9% of the molecule set), computing the lowest-energy isomer (local quench plus frequency calculation) at AM1 is between 91 and 1436 times faster than at DFT/basis1, and between 1204 and 34 425 times faster than at DFT/basis2. Local quench plus frequency calculations for the

lowest-energy isomer lasted between 2 and 73 seconds (~1 minute) at AM1, between 441 and 70 738 seconds (~20 hours) at DFT/basis1, and between 5 178 and 1 401 534 seconds (~16 days) at DFT/basis2. Thus, a conformational search through molecular dynamics (D_) followed by local quenches at DFT/basis1 was the best compromise to reach accuracy and a reasonable computational cost considering the large size of the database.

Temperature Effects

As said in **Materials and Methods – Global Exploration**, for each compound of the dataset, the five lowest-energy conformers were selected for local optimizations at each level of theory of this study, in particular at D_DFT/basis1. In this section, we highlight the temperature effects at D_DFT/basis1 level on the three following quantum descriptors: dipole moment, polarizability, and HOMO energy.

First, for 17 compounds, only one isomer was found. For 19 compounds only two isomers were found; for 16 compounds, 3 isomers were localized and for 25, 4. Finally, 5 isomers of low energies were found for 27 compounds. Among these 27 compounds, the fifth lowest-energy isomer abundance using a Boltzmann distribution at room temperature is at most 6.3% (diphenhydramine) and for 24 of these compounds, this abundance is less than 2%.

For the 104 dataset compounds, the polarizability and HOMO energy computed from the lowest-energy isomer differ by less than 2% from those resulting from Boltzmann weighted values obtained with the five lowest-energy structures. It can therefore be concluded that taking the Boltzmann distribution into account is not essential in the calculation of these two quantum descriptors.

However, if we now look at the values of the dipole moment, the effects of temperature are quite different (see Figure 5).

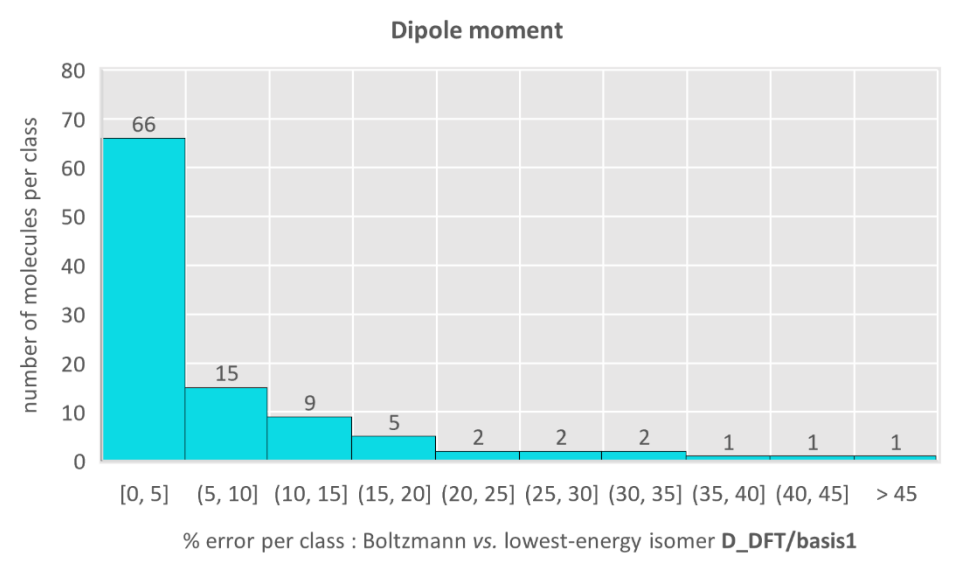

Figure 5. Percentage of errors by evaluating the dipole moment values using the lowest-energy isomer value instead of the Boltzmann averaged value (5 lowest-energy isomers) at room temperature at the D_DFT/basis1 level.

The difference between the lowest-energy value and the Boltzmann averaged value is less than 5 % for 66 compounds, between 5 and 10% for 15 compounds and between 10 and20% for 14 compounds. Finally, for 9 compounds, the error is greater than 20%: tetrabromobisphenolA (69%), omeprazole (44%), estriol (36%), gemfibrozil (34%), 17-ethinylestradiol (30%), risperidone (29%), metoprolol (26%), oxytetracycline (24%), mestranol (23%), and olaquindox (20%). TetrabromobisphenolA has two isomers with Boltzmann equiprobabilities (54% and 46%) but as already mentioned (**Quantum Descriptor Analysis**), the lowest-energy isomer of tetrabromobisphenolA has a small μ = 0.533 D (at D_DFT/basis1), whereas the second lowest-energy isomer exhibits a larger μ value 3.108 D (at D_DFT/basis1). Consequently, the Boltzmann weighted dipole moment value of 1.719 D is far from both isomer values. For the 8 other compounds, the observation is to a lesser extent the same: a wide range of variation of the dipole moment for all the conformers combined with non-negligible Boltzmann weights.

To correctly evaluate the dipole moment, Boltzmann distribution must be considered but to get correct polarizabilities and HOMO energies, the values obtained for the lowest-energy conformer is sufficient. As quantum descriptor calculations were performed for the five lowest-energy isomers, we suggest adding the Boltzmann average dipole moment in the Typol database.

Quantum Descriptor Analysis

In this section, we seek to show that the information carried by the 3D quantum descriptors is not already contained in descriptors simpler to calculate, which do not require the determination of the lowest-energy conformer followed by quantum chemistry calculations. Thus, the distribution functions

of the 3D quantum descriptors computed with the D_DFT/basis2 strategy, are discussed regarding non-quantum descriptors, *i.e.*, descriptive or based on 2D or 3D structural formula (Table SII). For example, we will look for a link: i) between the dipole moment and the number of heteroatoms (nHet) of the molecule; ii) between the polarizability and the molecular weight (MW); iii) between the ionization potential and the number of heteroatoms (nHet) or the number of aromatic bonds (nAB).

The dipole moment (μ) results from the vectorial linear combination of the bond and lone pair μ present in the molecule. The greater the difference in the electronegativity between two atoms, the more the bond is polarized and the greater the bond dipole moment (bond μ). Consequently, the molecules containing heteroatoms, N, O, S, F, Cl, Br and I, which are more electronegative than C or H, will have more polarized bonds and thus, non-zero bond μ. However, dipole moment values are not completely determined by the number of heteroatoms in a molecule because of the tremendous influence of the molecule conformation in the result of the vectorial linear combination of bond μ to obtain the μ of the molecule. In the molecule set, μ goes from 0.253 D for estriol to 11.825 D for norfloxacin (Figure 6).

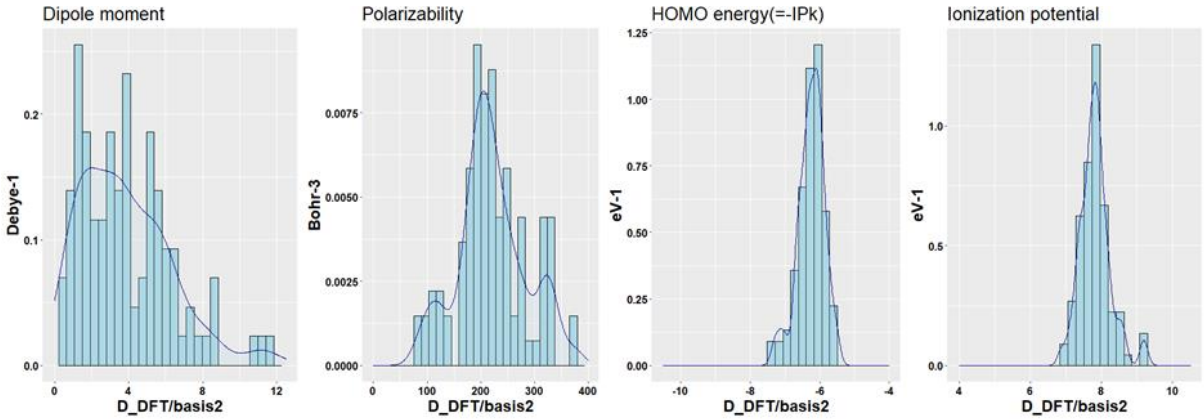

Figure 6. Distribution functions of the following quantum descriptors calculated at the D_DFT/basis2 level of theory: dipole moment (Debye), polarizability ($Bohr^3$), HOMO energy (= $-IP_K$) (eV) and IP, ionization potential (eV). Only the set of molecules with indices **1**, **2**, **3** and **4** (100 molecules) was used to produce the graphs. The indices are defined in **Results and Discussion**.

Fifty-seven molecules have a μ between 0.253 D and 3.8 D, the mean value for the dipole moment. The μ values are not normally distributed (Figure 6). Consequently, in Table III, mean and median do not correspond. Only seven molecules have a μ > 8.0 D and are part of the fluoroquinolones having the 2D formula shown on Figure 7 and differing by R1 and R2 groups. Members of the fluoroquinolones contain at least one fluorine atom, which is the most electronegative element of the whole periodic classification.

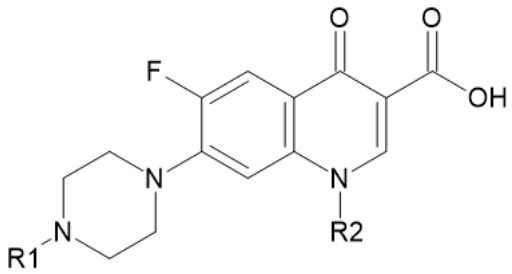

Figure 7. Fluoroquinolones 2D formula: the members of this family differ by R1 and R2 groups.

The great polarity of the C—F bond can partly explain the large values of μ in the fluoroquinolones. As expected, μ values are not completely determined by the number of heteroatoms (nHet), for instance, the lowest-energy isomer of tetrabromobisphenolA has a small μ of 0.757 D although it has four bromine and two oxygen atoms whereas the second lowest-energy isomer of this compound exhibits a larger μ value of 3.236 D as mentioned previously in **Temperature Effects**.

The polarizability (α) is the aptitude of the electronic cloud of a molecule to deform when an electric field is applied. It depends on the size of the electronic cloud and thus, on the number of electrons within the molecule. For an atom ${}^{A}_{Z}X$, the number of electrons Z and the atomic weight A are clearly related. Consequently, for a molecule, α increases with the molecular weight (MW). Looking at the distribution function for α on Figure 6, ten molecules belong to the eleven lowest α values (< 135 Bohr^3) and the eleven lowest MW values (< 185 g/mol) and have less than twenty-seven atoms. At the same time, the twelve highest MW values (> 414 g/mol) share nine molecules with the twelve highest α values (> 319 Bohr^3). Both extreme values are found for the same molecules for α and MW: the minima are for ortho-cresol (108.15 g/mol, 86.44 Bohr^3); the maxima for iopromide (791.15 g/mol, 375.11 Bohr^3). Moreover, looking at the molecules around the average values (av) of MW and α ($av \pm \frac{1}{3}\sigma$, σ the standard deviation), twenty-three are in common over thirty-two molecules for α and over thirty-one for MW. In fact, MW and α distribution functions are *quasi* stackable. Moreover, as polarizabilities are little influenced by the conformation of the molecules, polarizabilities were represented versus MW for the whole set of molecules (except index **0**) (Figure 8).

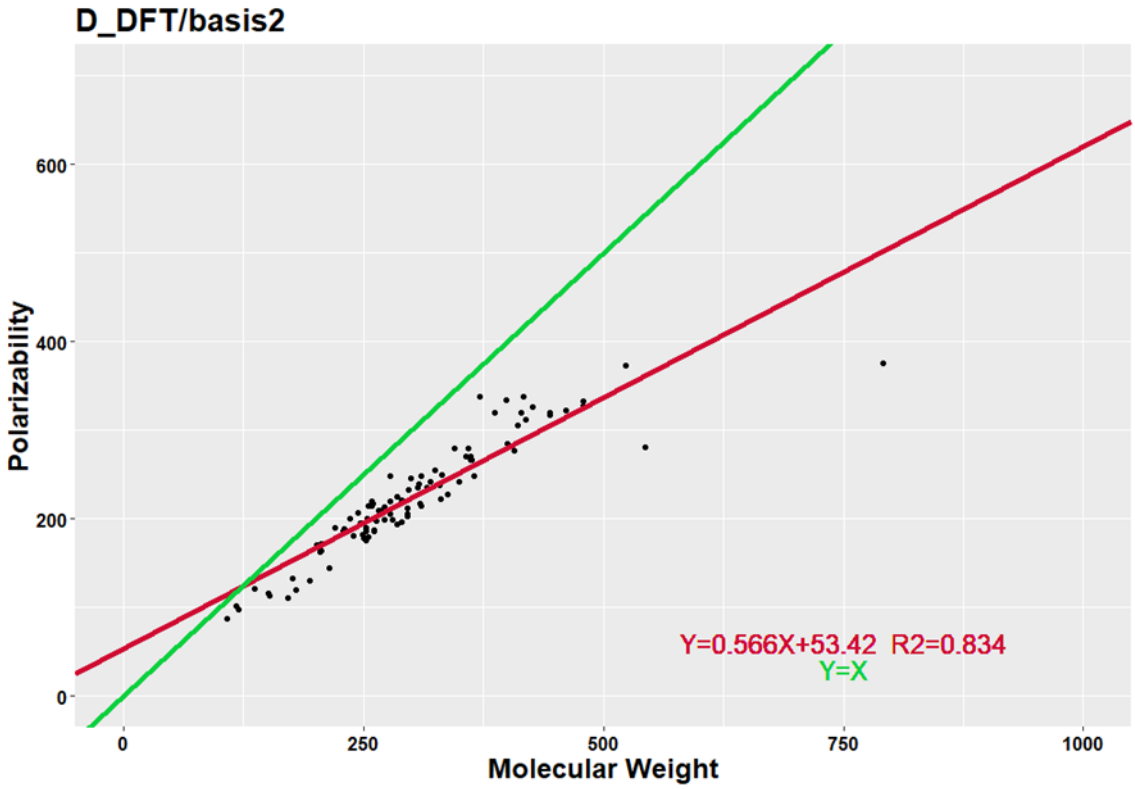

Figure 8. Polarizabilities ($Bohr^3$) at D_DFT/basis2 level versus molecular weight (MW) values (g/mol). The equation, y=ax+b, of the linear regression line is written in red with the corresponding R^2 regression coefficient, while the green straight line represents the first bisector: y=x. Only the set of molecules with indices **1**, **2**, **3** and **4** (100 molecules) was used to produce the graphs. The indices are defined in **Results and Discussion**.

Linear regression leads to the following equation: α ($Bohr^3$) = 0.566 MW (g/mol) + 53.42; with an acceptable dispersion (R^2 = 0.834). Two points were clearly more distant to the straight line: iopromide (791.15 g/mol, 375.11 $Bohr^3$) and tetrabromobisphenolA (543.87 g/mol, 280.17 $Bohr^3$). Iopromide is the only molecule of the set containing iodine and tetrabromobisphenolA, the only molecule containing bromine (Figure 8). Iodine and bromine are the heaviest elements present in the set of molecules under study. The greatest dispersion for both molecules could be explained by the quality of the basis set used for these two elements: only basis1 was used as basis2 was not available (α are then underestimated). Moreover, we did not consider scalar relativistic effects with core pseudopotentials, which could be harmful for these two elements. Anyway, knowing MW for a PPCP molecule, we can predict its polarizability value with an acceptable accuracy (R^2 = 0.834) *via* the equation: α ($Bohr^3$) = 0.566 MW (g/mol) + 53.42.

For the ionization potential, we have two objectives here. The first one is to relate this potential to the descriptors nAB and nHet and to highlight that the information carried by the ionization potential is not already contained in these two descriptors. The second objective is to show that the calculation of the ionization potential is improved if the electronic reorganization is considered: IP *versus* IP_K (see **Materials and Methods**). The ionization potential is the minimal energy to extract one electron from a molecule. If IP differs from IP_K, IP gives a more reliable value as it takes electronic reorganization into

account. Figure 9 presents IP as a function of IP_K both computed at D_DFT/basis2 (a) or D_DFT/basis1 (b). For both linear regression lines, the slopes are close to one: a=1.03 (D_DFT/basis2) and a=1.021 (D_DFT/basis1).

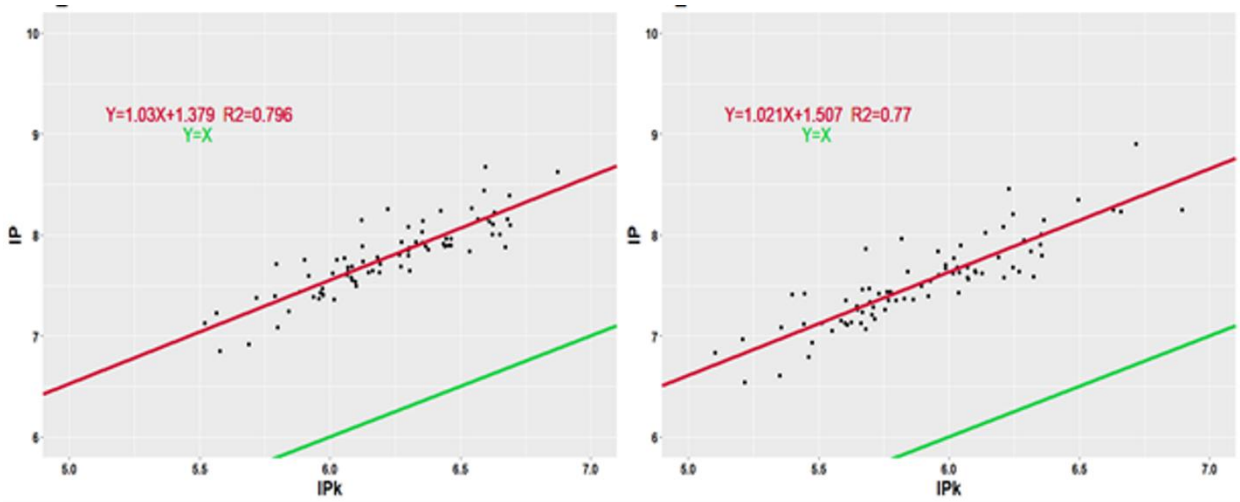

Figure 9. At both D_DFT/basis2 (a) and D_DFT/basis1 (b) levels, straight lines in red are confronting IP (eV) values on the vertical axis to IP_K (= - HOMO energy) (eV) values. On both graphs, the equation, y=ax+b, of the linear regression line is written in red with the corresponding R^2 regression coefficient, while the green straight line represents the first bisector: y=x. (a) Only the set of molecules with indices **1**, **2**, **3** and **4** (100 molecules) was used to produce the graphs. (b) All the set of molecules was used to produce the graphs: indices **0**, **1**, **2**, **3** and **4** (104 molecules). The indices are defined in **Results and Discussion**.

Thus, the lines are almost parallel to the first bisector. IP_K underestimates IP and shifting IP_K by b=1.379 eV (D_DFT/basis2) and by b=1.507 eV (D_DFT/basis1) gives almost the value of the corresponding IP. Moreover, the dispersion observed (R^2=0.796, 0.77 respectively) indicates that the electronic reorganization depends on the molecule under interest. The indirect method is then recommended to obtain more accurate IP values. On Figure 6, both IP and HOMO energy distribution functions are represented. Looking at the molecules around the average values (av) of IP and HOMO energy ($av \pm \frac{1}{3}\sigma$, σ the standard deviation), 15 are in common over 36 molecules for IP, and over 25 for HOMO energy. For the extreme values: (i) eight molecules belong to both the ten lowest HOMO energies and the ten highest IP values; (ii) seven molecules belong to both the ten highest HOMO energies and the ten lowest IP values. Overall, as similar patterns are observable for IP and IP_K (=-HOMO energy) distribution functions, we will thus focus on the description of IP. For the 100 molecules under study, IP values are going from 6.855 eV (tamoxifen) to 9.237 eV (metrodinazole) with an average value of 7.832 eV (median = 7.810 eV). The 36 molecules with IP values around the average, have IP values between 7.693 (pyrimethamine) and 7.979 eV (iopromide). When the electron is extracted from the HOMO, this orbital is either a heteroatom lone-pair or a π orbital. For instance, among the largest IP, the electron is extracted from the π HOMO for aspirin, and from the carbonyl oxygen lone pair for acetophenone. For metrodinazole, the HOMO of the neutral molecule is the hydroxyl oxygen lone pair whereas, in the cation, the depopulated orbital is a π orbital delocalized over the imidazole cycle. The

electronic reorganization is evidently important between the neutral and cationic forms, in this case, Koopman's Theorem fails. Finally, we tried to relate IP and descriptive descriptors as nHet (number of heteroatoms) or nAB (number of aromatic bonds) but no clear correlation was found.

In the following, we intend to connect quantum descriptors with non-quantum descriptors using a partial least square regression (PLS) to evidence the possible correlations between both types of descriptors. A PLS was performed considering the non-quantum descriptors not depending on the conformation of the molecule as the predictive variables (X) (see Table SII) and the quantum descriptors as predicted variables (Y). The non-quantum descriptors were obtained from the Dragon software while the quantum descriptors used were calculated with the D_DFT/basis2 method. The number of PLS components was four. Components 1 and 2 were the ones collecting the highest explained variance. For the predictive variables (X), the explained variance on component 1 was 26.5% and 10.4% for component 2. For the predicted variables (Y), the explained variance was 11.1% and 10.9% on components 1 and 2, respectively. The explained variance is low on both components for the predictive and the predicted variables. Thus, the information provided by quantum descriptors is poorly described by non-quantum descriptors. This fact constitutes a first proof of the importance of considering quantum descriptors in the TyPol database to best describe the molecules and hope to predict their environmental behavior.

On Figure 10, the correlation circle showed that the weight of the component 1 came from the molecular weight (MW), the number of hydrogen acceptor (nHAcc), the number of heteroatoms (nHet), the number of hydrogen donor (nHDon) and the number of hydroxyl groups (nOH). The weight of component 2 is carried by the number of aromatic bonds (nAB) and the number of benzene type rings (nBnz) (Figure 10). The Cluster Image Map (CIM) was also constructed from the PLS regression data. The CIM allows to obtain the correlation level between the predictive and the predicted variables according to the set of variables.

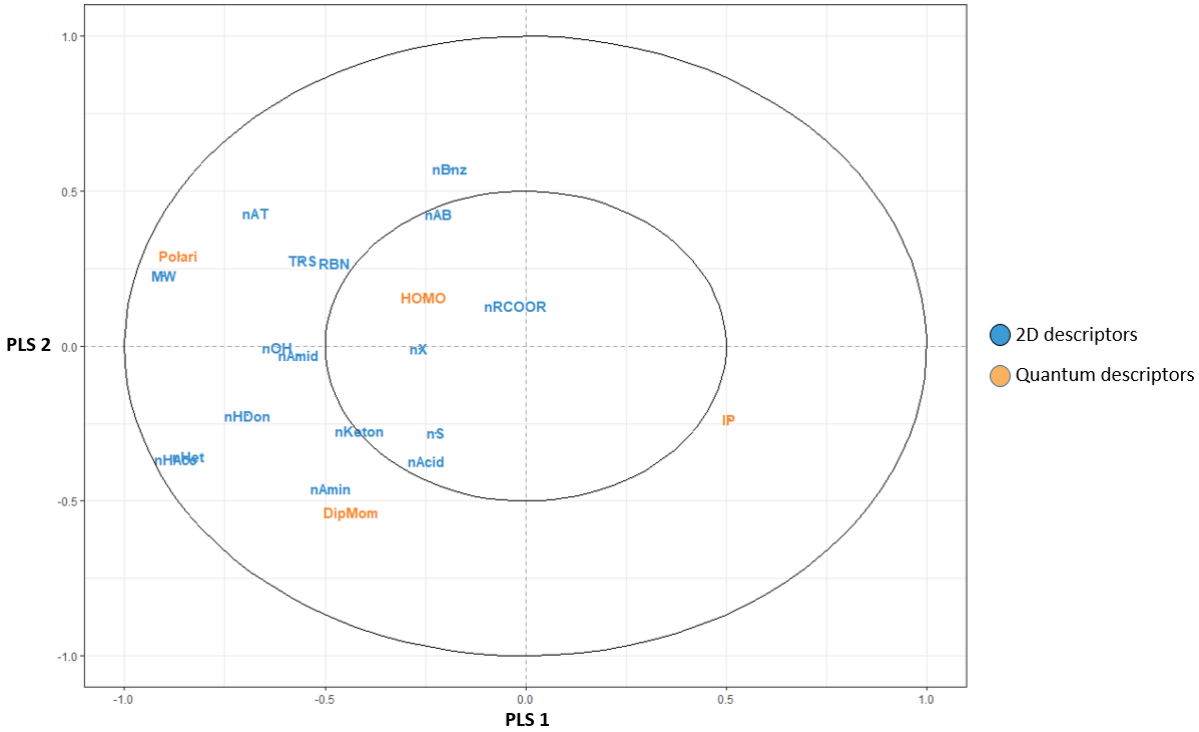

Figure 10. Circles of correlations of the non-quantum molecular descriptors (in blue) and '3D quantum descriptors' (in orange) variables on the two main components of the PLS (PLS1 and PLS2). HOMO stands for HOMO energy, IP for ionization potential, Polari for polarization and DipMom for dipole moment. See Table SII for the description of the non-quantum molecular descriptors.

The HOMO energy was the least explained quantum descriptor (Figure 10). The IP seems to be negatively correlated with both descriptors nAB and nBnz according to the CIM of component 2. IP is also negatively correlated to nHAcc, nHet and MW on the component 1 (Figure 10). The dipole moment, which tends to the lower left part of the correlation circle, is positively correlated with the amine number (nAmin) and ketone number (nKeton), and negatively correlated with nAB and nBnz. Finally, polarizability is the quantum descriptor that correlates best with the descriptors (Figure 10). This quantum descriptor is related to MW, nHAcc, nHet, Total Ring Size (TRS) and the number of rotatable bonds (RBN).

The strongest correlations established by the PLS between quantum and non-quantum descriptors had all been anticipated but remain very weak given the explained variances. Therefore, the information carried by the quantum descriptors (dipole moment, polarizability, HOMO energy and ionization potential) is not redundant with that carried by the non-quantum descriptive, 2D and 3D descriptors. The intrinsic properties of the molecule are better described when the quantum descriptors are included.

Conclusion

As a conclusion, the importance of doing a comprehensive conformational search through molecular dynamics was characterized. Investigating the quality and efficiency of various levels of theory (AM1,

DFTB and DFT) for computing quantum descriptors, namely dipole moment, polarizability, ionization potential and HOMO energy, we propose a strategy, the so-called D_DFT/basis1, as a good compromise between accuracy and computational cost. It consists in an exhaustive MD conformational search followed by a local optimization at B3LYP/6-31G*. Moreover, we showed that dipole moment values are not completely determined by the number of heteroatoms in a molecule, indeed, the conformation of the molecule has a tremendous influence on the dipole moment value. On the contrary, knowing the molecular weight of a molecule allows to predict with an acceptable accuracy its polarizability. At the same time, ionization potential values are not correlated with the number of heteroatoms or the number of aromatic bonds in the compound. Finally, information bared by quantum descriptors is not redundant with the one bared only by the non-quantum descriptive, 2D and 3D descriptors. Therefore, quantum descriptors (dipole moment, polarizability, HOMO energy, ionization potential) should be considered into TyPol database. At present, the quantum descriptors calculated at the D_DFT/basis1 level are being calculated for all 500 organic contaminants in the TyPol database. We showed that averaging the quantum descriptors values obtained for the lowest-energy isomers with a Boltzmann distribution provides values very close to those of the most stable isomer for the polarizabilities and the HOMO energies. On the opposite, the dipole moments can be strongly affected by the introduction of higher energy isomers contributions. Once the database has been updated, we will be able to test the consequences of these improvements on the classifications already published,[52] but above all to consider new and more ambitious projects. However, the improvement of the base is continuous. New descriptors can be integrated describing, for example, solvent effects: a first step towards quantum descriptors directly linked to the behavior of a contaminant in the environment.

Supporting Information Summary

More details on the computational chemistry methods are given for DFT and DFTB (**1.**). Similarly, further information about ionization potential calculations is presented (**2.c.**). The molecule set of 104 PPCP is separated into 5 groups further details about those groups: indices, exclusivity, percentages; are given in Table SI. The list of the 20 non-quantum descriptors from Dragon software used in this work are gathered in Table SII. A comparison of 3 quantum-based 3D descriptors calculated at D_DFT/basis1 (chosen strategy) and at H_AM1 (presently in the TyPol database) is represented on Figure S1. An archive file is provided including the most stable isomer structures obtained with the chosen strategy, D_DFT/basis1.

Acknowledgement

This work was granted access to the HPC resources of CALMIP supercomputing center under the allocation 2016-[P1222].

Funding Information

We would like to thank ADEME (French Agency for Ecological Transition) and INRAE (French National Research Institute for agriculture, food, and environment) for the PhD grant of Kevin Bonnot and OFB (French Office for Biodiversity) for its financial and scientific supports.

Keywords

Database

DFT

DFTB

Molecular descriptors

QSAR

673 **References**

674 [1] C. G. Daughton, T. A. Ternes, *Environmental Health Perspectives* **1999**, *107*, 907–938.
675 [2] J. Kagle, A. W. Porter, R. W. Murdoch, G. Rivera-Cancel, A. G. Hay, in *Advances in Applied*
676 *Microbiology*, Elsevier, **2009**, pp. 65–108.
677 [3] D. C. G. Muir, P. H. Howard, *Environ. Sci. Technol.* **2006**, *40*, 7157–7166.
678 [4] J. C. Dearden, P. Rotureau, G. Fayet, *SAR and QSAR in Environmental Research* **2013**, *24*, 279–
679 318.
680 [5] G. Fayet, P. Rotureau, L. Joubert, C. Adamo, *Journal of Molecular Modeling* **2010**, *16*, 805–812.
681 [6] L. Mamy, D. Patureau, E. Barriuso, C. Bedos, F. Bessac, X. Louchart, F. Martin-Laurent, C. Miege,
682 P. Benoit, *Critical Reviews in Environmental Science and Technology* **2015**, *45*, 1277–1377.
683 [7] L. Mamy, E. Barriuso, B. Gabrielle, *Pest Management Science* **2005**, *61*, 905–916.
684 [8] R. Servien, L. Mamy, Z. Li, V. Rossard, E. Latrille, F. Bessac, D. Patureau, P. Benoit, *Chemosphere*
685 **2014**, *111*, 613–622.
686 [9] *Dragon 7.0, Software for Molecular Descriptor Calculation.*, Talete S.R.L., **2017**.
687 [10] M. Karelson, V. S. Lobanov, A. R. Katritzky, *Chem. Rev.* **1996**, *96*, 1027–1044.
688 [11] A. Soyemi, T. Szilvási, *J. Phys. Chem. A* **2022**, *126*, 1905–1921.
689 [12] D. Hait, M. Head-Gordon, *Phys. Chem. Chem. Phys.* **2018**, *20*, 19800–19810.
690 [13] D. Hait, M. Head-Gordon, *J. Chem. Theory Comput.* **2018**, *14*, 1969–1981.
691 [14] A. R. Katritzky, S. Perumal, R. Petrukhin, E. Kleinpeter, *J. Chem. Inf. Comput. Sci.* **2001**, *41*, 569–
692 574.
693 [15] A. R. Katritzky, L. Pacureanu, D. Dobchev, M. Karelson, *J Mol Model* **2007**, *13*, 951–963.
694 [16] P. Hohenberg, W. Kohn, *Phys. Rev.* **1964**, *136*, B864–B871.
695 [17] W. Kohn, L. J. Sham, *Phys. Rev.* **1965**, *140*, A1133–A1138.
696 [18] C. Lee, W. Yang, R. G. Parr, *Phys. Rev. B* **1988**, *37*, 785–789.
697 [19] A. D. Becke, *The Journal of Chemical Physics* **1993**, *98*, 5648–5652.
698 [20] M. M. Francl, W. J. Pietro, W. J. Hehre, J. S. Binkley, M. S. Gordon, D. J. DeFrees, J. A. Pople, *The*
699 *Journal of Chemical Physics* **1982**, *77*, 3654–3665.
700 [21] V. A. Rassolov, M. A. Ratner, J. A. Pople, P. C. Redfern, L. A. Curtiss, *J. Comput. Chem.* **2001**, *22*,
701 976–984.
702 [22] M. N. Glukhovtsev, A. Pross, M. P. McGrath, L. Radom, *The Journal of Chemical Physics* **1995**, *103*,
703 1878–1885.
704 [23] A. D. McLean, G. S. Chandler, *The Journal of Chemical Physics* **1980**, *72*, 5639–5648.
705 [24] M. P. McGrath, L. Radom, *The Journal of Chemical Physics* **1991**, *94*, 511–516.
706 [25] L. A. Curtiss, M. P. McGrath, J. Blaudeau, N. E. Davis, R. C. Binning, L. Radom, *The Journal of*
707 *Chemical Physics* **1995**, *103*, 6104–6113.
708 [26] F. Bessac, S. Hoyau, *Computational and Theoretical Chemistry* **2011**, *966*, 284–298.
709 [27] F. Bessac, S. Hoyau, *Computational and Theoretical Chemistry* **2013**, *1022*, 6–13.
710 [28] M. J. Frisch, G. W. Trucks, H. B. Schlegel, G. E. Scuseria, M. A. Robb, J. R. Cheeseman, G. Scalmani,
711 V. Barone, G. A. Petersson, H. Nakatsuji, X. Li, M. Caricato, A. Marenich, J. Bloino, B. G. Janesko,
712 R. Gomperts, B. Mennucci, H. P. Hratchian, J. V. Ortiz, A. F. Izmaylov, J. L. Sonnenberg, D. Williams-
713 Young, F. Ding, F. Lipparini, F. Egidi, J. Goings, B. Peng, A. Petrone, T. Henderson, D. Ranasinghe,
714 V. G. Zakrzewski, J. Gao, N. Rega, G. Zheng, W. Liang, M. Hada, M. Ehara, K. Toyota, R. Fukuda, J.
715 Hasegawa, M. Ishida, T. Nakajima, Y. Honda, O. Kitao, H. Nakai, T. Vreven, K. Throssell, J. A.
716 Montgomery, Jr., J. E. Peralta, F. Ogliaro, M. Bearpark, J. J. Heyd, E. Brothers, K. N. Kudin, V. N.
717 Staroverov, T. Keith, R. Kobayashi, J. Normand, K. Raghavachari, A. Rendell, J. C. Burant, S. S.
718 Iyengar, J. Tomasi, M. Cossi, J. M. Millam, M. Klene, C. Adamo, R. Cammi, J. W. Ochterski, R. L.
719 Martin, K. Morokuma, O. Farkas, J. B. Foresman, D. J. Fox, **n.d.**
720 [29] D. Porezag, T. Frauenheim, T. Köhler, G. Seifert, R. Kaschner, *Phys. Rev. B* **1995**, *51*, 12947–12957.
721 [30] G. Seifert, D. Porezag, T. Frauenheim, *Int. J. Quantum Chem.* **1996**, *58*, 185–192.
722 [31] M. Elstner, D. Porezag, G. Jungnickel, J. Elsner, M. Haugk, T. Frauenheim, S. Suhai, G. Seifert, *Phys.*
723 *Rev. B* **1998**, *58*, 7260–7268.

[32] Y. Yang, H. Yu, D. Uork, Q. Cui, M. Elstner, *J. Phys. Chem. A* **2007**, *111*, 10861–10873.
[33] M. Gaus, Q. Cui, M. Elstner, *Journal of Chemical Theory and Computation* **2011**, *7*, 931–948.
[34] M. Gaus, A. Goez, M. Elstner, *Journal of Chemical Theory and Computation* **2013**, *9*, 338–354.
[35] L. Zhechkov, T. Heine, S. Patchovskii, G. Seifert, H. A. Duarte, *J. Chem. Theory Comput.* **2005**, *1*, 841–847.
[36] H. A. Witek, K. Morokuma, A. Stradomska, *The Journal of Chemical Physics* **2021**, *121*, 5171–5178.
[37] T. Heine, M. Rapacioli, S. Patchkovskii, J. Frenzel, A. Koster, P. Calaminici, H. A. Duarte, S. Escalante, R. Flores-Moreno, A. Goursot, J. Reveles, D. Salahub, A. Vela, *deMonNano, http://demon-nano.ups-tlse.fr/* **2009**.
[38] M. J. S. Dewar, W. Thiel, *J. Am. Chem. Soc.* **1977**, *99*, 4899–4907.
[39] M. J. S. Dewar, E. G. Zoebisch, E. F. Healy, J. J. P. Stewart, *J. Am. Chem. Soc.* **1985**, *107*, 3902–3909.
[40] A. Banerjee, N. Adams, J. Simons, R. Shepard, *J. Phys. Chem.* **1985**, *89*, 52–57.
[41] J. Baker, *J. Comput. Chem.* **1986**, *7*, 385–395.
[42] P. Culot, G. Dive, V. H. Nguyen, J. M. Ghuysen, *Theoret. Chim. Acta* **1992**, *82*, 189–205.
[43] X. Li, M. J. Frisch, *J. Chem. Theory Comput.* **2006**, *2*, 835–839.
[44] T. Koopmans, *Physica* **1934**, *1*, 104–113.
[45] D. Danovich, *Journal of Molecular Structure: THEOCHEM* **1997**, *401*, 235–252.
[46] P. Politzer, F. Abu-Awwad, *Theoretical Chemistry Accounts: Theory, Computation, and Modeling (Theoretica Chimica Acta)* **1998**, *99*, 83–87.
[47] S. Hamel, P. Duffy, M. E. Casida, D. R. Salahub, *Journal of Electron Spectroscopy and Related Phenomena* **2002**, *123*, 345–363.
[48] R. Vargas, J. Garza, A. Cedillo, *J. Phys. Chem. A* **2005**, *109*, 8880–8892.
[49] J. Luo, Z. Q. Xue, W. M. Liu, J. L. Wu, Z. Q. Yang, *J. Phys. Chem. A* **2006**, *110*, 12005–12009.
[50] T. Tsuneda, J.-W. Song, S. Suzuki, K. Hirao, *The Journal of Chemical Physics* **2010**, *133*, 174101.
[51] James J. P. Stewart, Stewart, *MOPAC2009 Computational Chemistry*, Colorado Springs, CO, USA, **2009**.
[52] P. Benoit, L. Mamy, R. Servien, Z. Li, E. Latrille, V. Rossard, F. Bessac, D. Patureau, F. Martin-Laurent, *Science of The Total Environment* **2017**, *574*, 781–795.

ToC

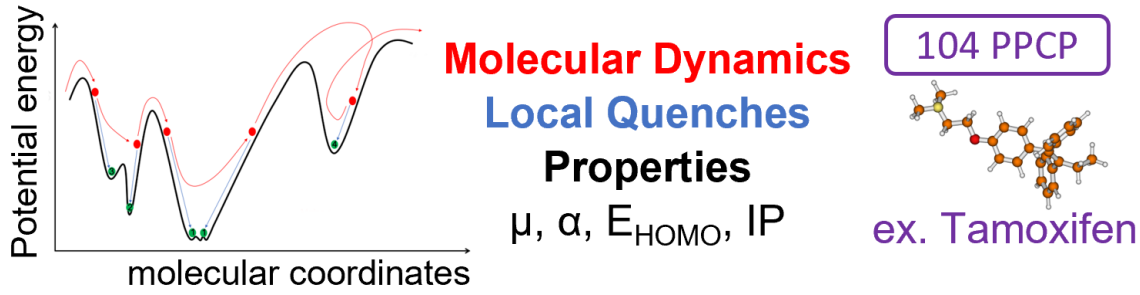

For 104 pharmaceuticals and personal care products (PPCP), four quantum-based 3D descriptors (electric dipole moment, polarizability, HOMO energy and ionization potential) were calculated using different computational chemistry strategies combining a molecular dynamics global exploration with local quenches within different frameworks (semi-empirical, DFTB, DFT).